Magnetic Field Sensing Based on Multimode Fiber Specklegrams

Run-ze Zhu, Sheng-jie Wan, Yi-feng Xiong, Hao-gong Feng, Ye Chen, Yan-qing Lu, and Fei Xu

***Abstract*—We demonstrate a fiber magnetic field sensor based on multimode fiber specklegrams. The magnetic field is detected by measuring the change of speckle patterns with digital correlation technology. When the magnetic induction increases by 50 mT, the response of correlation coefficient is more than 0.35. The sensitivity of the sensor is 0.00705 mT^{-1} for the magnetic field range of 50–100 mT, and the resolution is 0.284 mT. The temperature cross sensitivity is studied by establishing the sensing matrix. In addition, dynamic range expansion and magnetic field direction sensing are explored as the application extensions of this kind of sensor.**

***Index Terms*—Dynamic range, fiber specklegram sensor, magnetic field direction, magnetic field sensing, temperature cross sensitivity.**

I. Introduction

MAGNETIC field sensors play an important role in various industries such as medicine, geophysics, energy survey and so on. Compared with other magnetic sensors, fiber magnetic field sensors have the advantages of low-cost, small size and high reliability. Magnetic fluid (MF) is a kind of stable colloidal liquid composed of magnetic solid particles with a diameter of less than 10 nm, a carrier liquid (also known as media) and surfactant. In the external magnetic field, it shows excellent magneto-optical properties such as tunable refractive index, Faraday effect and thermal lens effect. In recent years, the fiber-optic vector magnetic field sensors based on MF have attracted wide research attention and most of them obtain the magnetic field information by analyzing the optical spectrum. For example, grating-based sensors [1], [2] and interferometric based sensors [3]–[5] have been designed with MF acting as the modified cladding. However, for directional detection, it is often necessary to fabricate asymmetric structures on optical fiber sensors, for example, by femtosecond laser microfabrication [6], side polishing [7] and dislocation fusion [8], which increases the difficulty and cost of sensor manufacturing and reduces the robustness of the device.

Optical fiber specklegram sensors (FSSs) are also a category of optical fiber sensors. When a coherent light propagates in a multimode fiber (MMF), an output speckle pattern is generated that results from inter-modal interference between all guided modes in the fiber. Because the spatio-temporal characteristics of speckle field are affected by light guiding conditions, the change of speckle patterns can be correlated with the change of external environments. Moreover, different methods for analyzing the speckle changes have been proposed, including digital correlation technique [9], statistical analysis [10], and morphological image processing [11]. The sensitivity of FSSs is high, and it can be realized by relatively simple experimental devices with low costs. In the fiber speckle sensing system, light source, multimode optical fiber and camera are necessary, usually in combination with some auxiliary devices, such as camera lens, objective lens, collimator and so on. The applications of FSSs have been reported to measure different physical quantities, concerning refractive index (RI) [9], strain [12], displacements [13], vibration [14], temperature [15], bending recognition [16], deformation [17] and so on. In addition, speckle sensing is also reported to be applied in biochemical measurements [18], multiplexed sensor [19], tactile sensing [20], force myography and human–robot interaction [21].

Magnetic field measurements with the fiber speckle pattern have been proposed in the last century [22]. Based on Faraday effect, the longitude magnetic field is calibrated by observing the rotation of the output speckle patterns of a low-mode fiber [23]. In addition, graphene and other materials can be used to control the rotation characteristics of the pattern [24]. This method is suitable for measuring the longitudinal magnetic field in the order of kOe.

In this work, we propose a new method of measuring magnetic field based on multimode fiber specklegrams, which has the potential to realize optical fiber magnetic field sensing with simple devices and low costs. The sensor has high sensitivity and good linear response to the change of magnetic field intensity and the temperature cross sensitivity is studied. In addition, dynamic range expansion and magnetic field direction sensing are explored as the application extensions of this kind of sensor.

II. Principle of Operation

When a coherent light is launched into a MMF, an output speckle pattern is formed at the fiber end face. The output speckle

Manuscript received January 6, 2021; revised February 26, 2021; accepted March 15, 2021. Date of publication March 18, 2021; date of current version June 2, 2021. This work was sponsored in part by the National Natural Science Foundation of China under Grants 61925502, 61535005, 62035006, and 62005118 and in part by the National Key R&D Program of China under Grants 2017YFA0303700 and 2017YFC1403803. *(Run-ze Zhu and Sheng-jie Wan contributed equally to this work.) (Corresponding author: Ye Chen and Fei Xu.)*

The authors are with the College of Engineering and Applied Sciences, Nanjing University, Nanjing 210093, China (e-mail: 759006137@qq.com; 151190085@smail.nju.edu.cn; 309896366@qq.com; dz1934002@smail.nju.edu.cn; yechen@nju.edu.cn; yqlu@nju.edu.cn; feixu@nju.edu.cn).

Color versions of one or more figures in this article are available at https://doi.org/10.1109/JLT.2021.3067332.

Digital Object Identifier 10.1109/JLT.2021.3067332

pattern is mainly caused by the interference of different modes in MMF. The random distribution of speckle field is determined by the intensity distribution and relative phase of each mode. Therefore, the intensity distribution of output specklegrams projected over a *xy*-plane $I(x, y)$ can be expressed as (1) [25]:

$$I(x,y) = \sum_{s=0}^{N-1} \sum_{t=0}^{N-1} a_s a_t \exp[j(\varphi_s - \varphi_t)] \tag{1}$$

where N is the number of modes, and a and φ are the amplitude and phase of the s-th or t-th modes, respectively. According to (1), the speckle intensity distribution is highly affected by the phase deviation $\Delta\varphi = \varphi_{\mathrm{s}} - \varphi_{\mathrm{t}}$, making it very sensitive to the external perturbation and stimulation. In addition, the speckle field distribution is also affected by the coupling between the N modes, so the power change of the s-th mode is calculated by (2) [26]

$$\Delta P_s = \sum_{t=0}^{N-1} \kappa_{st}(P_s - P_t) \tag{2}$$

where P_s is the initial power and κ_{st} is the coupling coefficient. Since the distribution of speckle intensity depends on the phase difference between modes and mode coupling effects, the speckle field are drastically affected by the state of incident light and the placement of optical fiber, as well as by the disturbance and stimulation from external environment, including temperature, strain, bending, refractive index and so on. Some work has also studied the intrinsic characteristics of specklegrams and tried to predict and control the speckle patterns [27]–[29]. In this context, by applying a magnetic field to the magnetic fluid around the microfiber, we can achieve magnetic field sensing by measuring the change of the speckle patterns. At the same time, the speckle pattern carries two-dimensional information, which also provides the possibility for magnetic field direction sensing.

Digital correlation is a common method to evaluate speckle pattern change. Common parameters for evaluating speckle pattern variation mainly include inner product, contrast and correlation coefficient. Here, we use Pearson correlation coefficient as the parameter to evaluate the change of speckle patterns, which is not sensitive to the overall change of image brightness and has stronger robustness in comparison to other speckle processing methods [9], [30]. The calculation formula of correlation coefficient is shown in (3) [15], (3) shown at the bottom of this page, where H and V are the total number of horizontal and vertical pixels. $I_R(h,\ v)$ and $I_m(h,\ v)$ are, respectively, the intensities of the reference speckle pattern and measured speckle pattern recorded by the camera in different pixel coordinates. $\bar{I}_R$ and $\bar{I}_m$ are their mean values. The original value of correlation coefficient is between 0 and 1. With the change of external magnetic induction, the output speckle pattern gradually deviates from the reference pattern, which causes the correlation coefficient to deviate from 1.

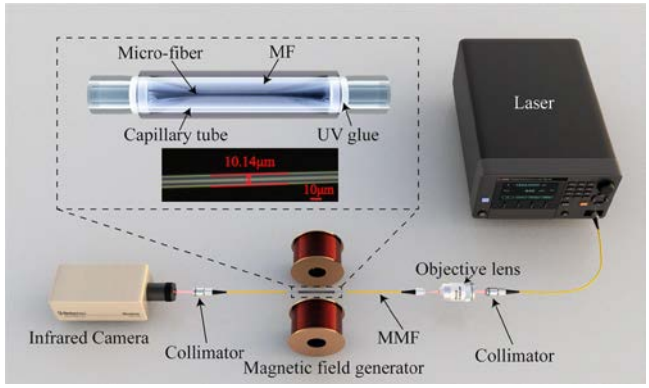

Fig. 1. Schematic of the experimental measurement setup; microscope image of microfiber sensor sample 3 and schematic of the MF-clad tapered microfiber magnetic field sensor in the black dotted box.

For FSSs based on digital correlation technology, the sensitivity of the sensor is usually calculated by correlation coefficient. In this paper, the sensitivity of this kind of sensor refers to the variation of the correlation coefficient when the external magnetic induction changes by 1 mT and the sensitivity unit of this magnetic field sensor is mT^{-1}.

III. Methodology

A. Sensor Fabrication

The sensors based on tapered microfiber are widely used because of their small size and high sensitivity. In this work, MMF (NUFERN MM-S105/125-12A) with core diameter of 105 μm was used to fabricate the microfiber magnetic field sensor. The structure diagram of the sensor is shown in the black dotted box in Fig. 1.

In general, the MMF was drawn by the flame brushing method. The heated fiber was stretched at a uniform speed through the motorized linear stages, forming a structure comprising a uniform taper waist and two transition regions, and each end of which is linked to an unstretched fiber by a conical section. Next, we packaged it in a capillary tube filled with MF by using UV-curing adhesive, which is mainly composed of acrylic resin. During UV curing, no strain is applied to the fiber. The inner diameter of the capillary is 0.5 mm and the length is 10 cm. After that, the multimode fiber can be directly used as a sensor for speckle sensing without additional fiber fusion, which is simpler and more convenient. In order to demonstrate different experiment purposes and sensing applications better, three samples with microfiber waist diameters of 14.1 μm,

$$C = \frac{\sum_{h=1}^{H}\sum_{v=1}^{V}\left[I_R(h,v) - \bar{I}_R\right]\left[I_m(h,v) - \bar{I}_m\right]}{\sqrt{\left\{\sum_{h=1}^{H}\sum_{v=1}^{V}\left[I_R(h,v) - \bar{I}_R\right]^2\right\}\left\{\sum_{h=1}^{H}\sum_{v=1}^{V}\left[I_m(h,v) - \bar{I}_m\right]^2\right\}}} \tag{3}$$

10.8 μm, and 10.14 μm were used, and the length of their waist areas is about 7 mm. The selection of structure parameters is mainly due to the trade-off between the evanescent field strength and the number of fiber modes. In our experiments, the water-based MF provided by BaseLine ChromTech Research Centre was employed. The nominal diameter of the nanoparticles (Fe_3O_4) is 10 nm and the RI of used MF is about 1.34 without magnetic field at the wavelength of 1550 nm. The total length of MMF is about 2 m.

B. Experimental Setup

The schematic diagram of the measuring device is shown in Fig. 1. The output light of tunable laser (Santec TSL710) is coupled into multimode fiber by the collimator (THORLABS F280APC-1550) and objective lens (20×), which is beneficial to excite higher-order modes. The part of microfiber sensor is placed in the magnetic field generator and the magnetic field can be changed by adjusting the current. The magnetic field direction is perpendicular to the optical fiber axis and the magnetic induction can be measured by a magnetometer. The output specklegrams of multimode fiber are expanded, collimated and projected to the infrared camera (Microviewer 7290A) through the fiber collimator (LBTEK FC1550-2-PC) and camera lens. In order to ensure the stability of the system, the multimode fiber sensor is fixed and the external environment interference is eliminated as much as possible. Except for special instructions, the experiment is carried out under the room temperature 23.7 °C.

C. Data Processing

The original images captured by the camera are 480 × 640 × 3 RGB images. For ease of processing, the RGB images are converted to grayscale images. In order to fully reduce the influence of image acquisition card and camera noise, 29 speckle patterns are collected and averaged for each magnetic induction. Then, the average speckle intensity is calculated by Matlab tools and the region of interest (ROI) is selected to calculate the correlation coefficient by (3). ROI size mainly depends on the size of the speckle pattern projected on the camera sensor and ROI is usually selected near the center of the speckle in this work. In most experiments, the speckle pattern without magnetic field is taken as the reference speckle.

IV. Results and Discussions

A. Single Wavelength Magnetic Field Sensing

Firstly, the sensor sample 1 was tested with the room temperature 23.7 °C and a magnetic field sensing experiment was carried out with 1550 nm laser. A square 67 × 67 pixels region with the blue border was selected as ROI, and the captured speckle pattern without magnetic field (0 mT) was used as the reference speckle pattern. The magnetic field generator was used to generate 0–150 mT magnetic field with 10 mT interval.

Fig. 2(a) shows the recorded speckle patterns of multimode fiber with magnetic inductions of 0 mT, 50 mT, 100 mT, and 150 mT and Fig. 2(b) shows the response to magnetic field.

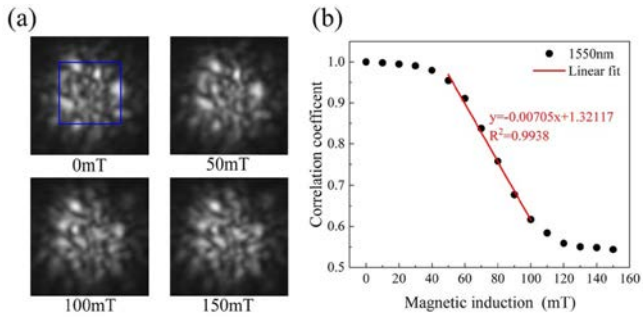

Fig. 2. The results of magnetic field sensing experiment at the wavelength of 1550 nm. (a) The averaged speckle patterns under the magnetic inductions of 0 mT, 50 mT, 100 mT, and 150 mT. The region in the blue border is selected as ROI. (b) Sensor responding to magnetic field at the wavelength of 1550 nm.

As shown in Fig. 2(b), after passing through a gentle region, the response enters the linear region and then tends to be gentle again. The dynamic range of the sensor is about 50–100 mT, and the sensitivity is 0.00705 mT^{-1}. The resolution of some fiber magnetic field sensors is calculated by the resolution of optical spectrum analyzer. In this work, the resolution of the sensor can be obtained by the resolution of the correlation coefficient, which is mainly affected by the noise of the camera and external noise. After repeated tests, the average correlation coefficient of speckle patterns taken continuously under the same conditions is more than 0.9980 and the resolution of the correlation coefficient is 0.0020. Therefore, the resolution of the sensor is 0.284 mT.

The trend of the response curve of magnetic field sensor is mainly affected by the properties of magnetic fluid. The principle analysis of its tunable RI responses to magnetic field has been reported widely in relevant works [3]–[7]. The change of MF's RI induced by magnetic field is designated as the agglomeration of magnetic nanoparticles in MF under external magnetic field. At a relatively low magnetic induction, the effect of magnetic field on MF is little. When a certain magnetic induction is applied, the nanoparticles start to agglomerate which leads to the increase of MF's RI. In the sufficiently high magnetic field, the change of MF's RI is close to the saturated state because all the nanoparticles agglomerate to form magnetic column. The maximum change of RI caused by magnetic field is estimated to be about 0.02. In addition, in our experiments, it is possible that magnetic fluid can cause the strain and bending of optical fiber with the change of magnetic field. Therefore, the change of speckle is because of not only the RI change but also the force.

B. Multi-wavelength Magnetic Field Sensing

Based on the single wavelength magnetic field sensing experiment, the multi-wavelength magnetic field response of the sensor sample 1 was measured by tunable laser. The speckle patterns of different magnetic inductions were recorded at wavelengths of 1510 nm, 1530 nm, 1550 nm, 1570 nm, and 1590 nm, respectively. The response curves of the sensor at each wavelength are shown in Fig. 3(a), and the linear fitting results of 50–100 mT magnetic field are calculated. Then, we explore the possibility

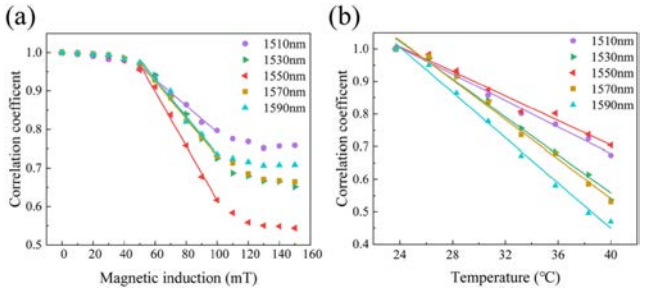

Fig. 3. The results of multi-wavelength magnetic field sensing experiment. (a) Magnetic field intensity response of the sensor sample 1 at the wavelengths of 1510 nm, 1530 nm, 1550 nm, 1570 nm, and 1590 nm. Five lines represent the fitting lines of the measurement results at different wavelengths. 1510 nm: $y = -0.00343x + 1.135$ $R^2 = 0.9880$; 1530 nm: $y = -0.00503x + 1.233$ $R^2 = 0.9903$; 1550 nm: $y = -0.00705x + 1.132$ $R^2 = 0.9938$; 1570 nm: $y = -0.00487x + 1.217$ $R^2 = 0.9977$; 1590 nm: $y = -0.00487x + 1.223$ $R^2 = 0.9877$; (b) Temperature response of the sensor sample 1 at the wavelengths of 1510 nm, 1530 nm, 1550 nm, 1570 nm, and 1590 nm. 1510 nm: $y = -0.02032x + 1.491$ $R^2 = 0.9911$; 1530 nm: $y = -0.02911x + 1.721$ $R^2 = 0.9895$; 1550 nm: $y = -0.01883x + 1.458$ $R^2 = 0.9815$; 1570 nm: $y = -0.03031x + 1.841$ $R^2 = 0.9885$; 1590 nm: $y = -0.03482x + 1.841$ $R^2 = 0.9938$.

of compensating temperature cross sensing by multi-wavelength responses.

Temperature cross sensitivity is a problem that must be considered in practical application of the sensors. The sensor sample 1 was heated on a constant temperature heating table and the speckle patterns were recorded from 23.7 °C to 40 °C at different wavelengths. With the change of temperature, the change of MF's refractive index, the thermal expansion of the capillary and UV glue, and the thermo-optic effect of the optical fiber are the main reasons for the change of speckle pattern. The speckle pattern recorded at room temperature (23.7 °C) was used as the reference pattern. The temperature response of the sensor was obtained by calculating the correlation coefficient, and the temperature sensitivities at different wavelengths were obtained by linear fitting. The measurement results are shown in Fig. 3(b).

The temperature sensitivities at five selected wavelengths are -0.02032 °C^{-1}, -0.02911 °C^{-1}, -0.01883 °C^{-1}, -0.03031 °C^{-1}, and -0.03482 °C^{-1}. The magnetic field sensitivities of the sample 1 at the selected wavelengths shown in Fig. 3(a) are $-0.00343\ \mathrm{mT}^{-1}$, $-0.00503\ \mathrm{mT}^{-1}$, $-0.00705\ \mathrm{mT}^{-1}$, $-0.00487\ \mathrm{mT}^{-1}$, and $-0.00487\ \mathrm{mT}^{-1}$, respectively. As shown in Fig. 3, the sensitivities of responses to the change of magnetic field and temperature are different at different wavelengths. For magnetic field and temperature sensing, the main reasons for the influence of different wavelengths on sensitivity are complex. Firstly, different wavelengths have great influence on the excitation modes in multimode fibers [31], and different modes have different contributions to the sensing sensitivity [32]–[35]. Secondly, due to the use of microfiber structure, considering the waist region diameter and transition region shape, mode coupling and mode loss occur, and the evanescent fields are different at different wavelengths [3], [36], causing the different responses to the change of magnetic field and temperature. In addition, both the fiber and MF have dispersion effect on the wavelength.

Inspired by the work of Haifeng Liu *et al.* [37], temperature cross sensitivity can be resolved by sensing matrix TM. As shown in (4), the sensing matrix TM is established by the sensitivities of temperature and magnetic field. In this way, temperature and magnetic induction can be measured simultaneously by TM and the changes of correlation coefficient. Therefore, the sensor can compensate for the temperature effects and measure magnetic field in a temperature changing environment.

$$\begin{bmatrix} \Delta c_1 \\ \Delta c_2 \\ \Delta c_3 \\ \Delta c_4 \\ \Delta c_5 \end{bmatrix} = TM \begin{bmatrix} \Delta B \\ \Delta T \end{bmatrix} = \begin{bmatrix} -0.00343\ \mathrm{mT}^{-1} & -0.02032^\circ\ \mathrm{C}^{-1} \\ -0.00503\ \mathrm{mT}^{-1} & -0.02911^\circ\ \mathrm{C}^{-1} \\ -0.00705\ \mathrm{mT}^{-1} & -0.01883^\circ\ \mathrm{C}^{-1} \\ -0.00487\ \mathrm{mT}^{-1} & -0.03031^\circ\ \mathrm{C}^{-1} \\ -0.00487\ \mathrm{mT}^{-1} & -0.03482^\circ\ \mathrm{C}^{-1} \end{bmatrix} \begin{bmatrix} \Delta B \\ \Delta T \end{bmatrix} \quad (4)$$

In this work, in order to adjust the wavelength conveniently, near infrared light source and camera are used. In fact, they can be replaced by visible light sources, filters, and cameras with lower costs.

C. Application Extensions of the Sensor

In this section, dynamic range expansion and magnetic field direction sensing are explored as the future discussion on the application developments of this kind of magnetic field sensor. In order to demonstrate different experiment purposes and sensing applications better, different sample sensors were used.

The dynamic range is usually limited due to the saturation of correlation coefficient, which is a prevalent problem in fiber speckle sensing. Most of the existing methods are based on speckle pattern division [38], morphological processing method [11] and algorithm compensation [39], which are suitable for the dynamic range limitation caused by too large difference between two patterns and have high complexity of image processing and algorithm. In this work, due to the difference of sensitivity and dynamic range of response curves at different wavelengths, it is possible to improve the dynamic range by multi-wavelength measurement combination. The sensor sample 2 was used for the dynamic range extension experiment.

As shown in Fig. 4(a), at the wavelengths of 1550 nm and 1570 nm, the linear dynamic range is about 20–70 mT. Due to the saturation of correlation coefficient, the linearity of the response curve is very low in the range of 20–120 mT and the R-squared obtained by linear fitting is only 0.8759 and 0.75018. However, when the measurement results at two wavelengths are subtracted, the fitting linear R-square of the response curve in the range of 20–120 mT exceeds 0.950, which means that the dynamic range is improved well. Similarly, as shown in Fig. 4(b), the linear fitting R-squared values of 1510 and 1590 nm response curves are 0.94789 and 0.95672 in the magnetic induction range of 30–110 mT. By adding the measured results at two wavelengths, the response curve is linearly fitted in the range of 30–110 mT,

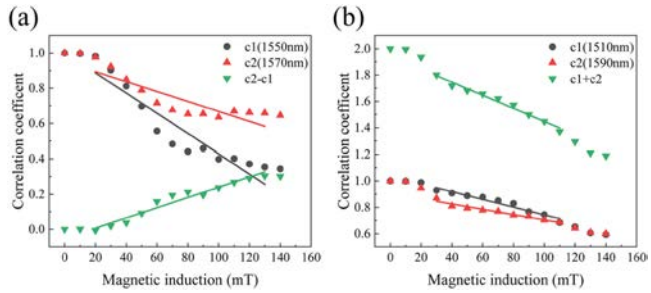

Fig. 4. The results of dynamic range extension experiment. (a) Magnetic field intensity responses of the sensor sample 2 at two wavelengths of 1550 nm and 1570 nm, and the result of subtraction. Three lines represent the fitting lines of three measurement results. c1: $y = -0.00573x + 1.002$ $R^2 = 0.8759$; c2: $y = -0.00282x + 0.9501$ $R^2 = 0.75018$; c2-c1: $y = 0.00291x$-0.05141 $R^2 = 0.9536$. (b) Magnetic field responses of the sensor sample 2 at two wavelengths of 1510 nm and 1590 nm, and the result of summation. Three lines represent the fitting lines of three measurement results. c1: $y = -0.00294x + 1.037$ $R^2 = 0.9479$; c2: $y = -0.00282x + 0.9501$ $R^2 = 0.9567$; c2 + c1: $y = -0.00497x1.9442$ $R^2 = 0.9803$.

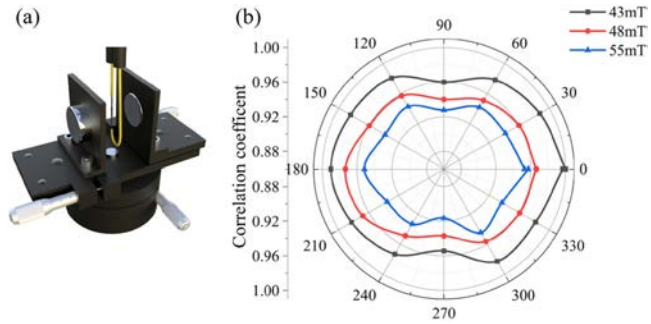

Fig. 5. (a) Schematic diagram of magnetic field rotating device. (b) Response of magnetic field direction sensing.

and the R square of the response curve is more than 0.980. Therefore, the measurement results combination of two wavelengths are demonstrated, which preliminarily confirms the possibility of improving dynamic range and linearity by combination of multi-wavelength measurements.

In addition to measuring the intensity of magnetic field, the method of fiber speckle sensing can also be used to calibrate the direction of magnetic field. Different from wavelength demodulation methods, FSS is based on two-dimensional image information. When the applied magnetic field direction changes, the output speckle pattern also changes, which makes it possible to analyze the magnetic field direction information by speckle sensing method.

The schematic diagram of magnetic field rotating device is shown in Fig. 5(a) and the sensor sample 3 was used for magnetic field direction sensing experiments. The speckle patterns were recorded under magnetic field of 43 mT, 48 mT, and 55 mT. The magnetic field direction angle varied from 0 to 360 degrees with 30 degrees interval. The speckle pattern at a predetermined 0-degree angle with 43 mT magnetic field was taken as the reference pattern.

As shown in Fig. 5(b), when the magnetic field direction angle is 0 degree and 90 degree respectively, the maximum difference of correlation coefficient is more than 0.04 and the trends of response curves are similar under different magnetic inductions. Considering that the correlation coefficient resolution is 0.0020, the magnetic field sensor has the ability to distinguish the magnetic field direction. Different from other magnetic field sensors, the proposed sensing method is based on the two-dimensional information of speckle images and the change of magnetic field direction can be observed and calibrated directly. The proposed sensor has direction-dependent property and has the potential to distinguish the direction of the magnetic field and further achieve vector magnetic field sensing through the optimization of the sensor and the improvement of the image processing method.

V. Conclusion

In summary, we demonstrate a fiber-optic magnetic field sensor based on multimode optical fiber specklegrams through digital correlation technology. The proposed method has the advantages of compact size and low costs. The sensor has the sensitivity of 0.00705 mT^{-1} in the magnetic field range of 50–100 mT with the resolution of 0.284 mT and the temperature cross sensitivity issue is studied by establishing the sensing matrix. Two application developments of this kind of magnetic field sensor are also discussed. The dynamic range and linearity can be improved by multi-wavelength measurement combination. Through the analysis of two-dimensional speckle image, the change of magnetic field direction can be observed and calibrated directly. Compared with the existing fiber magnetic field sensor, the proposed method is based on the analysis of two-dimensional speckle image and the proposed sensors use low-cost camera instead of wide spectrum light source or optical spectrum analyzer. Therefore, the sensor can be used for magnetic field measurements and has the potential to distinguish the direction of the magnetic field with simple devices and low costs, which is expected to apply to industry, navigation, military and other fields. The machine learning and correlation combination algorithm will be used to further improve the dynamic range and linearity by multi-wavelength measurement combination.

References

[1] Z. Zhang *et al.*, "Plasmonic fiber-optic vector magnetometer," *Appl. Phys. Lett.*, vol. 108, no. 10, pp. 101105-1–101105-4, Mar. 2016.
[2] W. Bao, X. Qiao, Q. Rong, and F. Chen, "Fiber-Optic vector magnetometer based on magnetic fluid and fiber bragg grating written on a multi-clad fiber," *IEEE Sensors J*, vol. 18, no. 18, pp. 7486–7491, Sep. 2018.
[3] L. Luo, S. Pu, J. Tang, X. Zeng, and M. Lahoubi, "Reflective all-fiber magnetic field sensor based on microfiber and magnetic fluid," *Opt. Exp.*, vol. 23, no. 14, pp. 18133–18142, Jul. 2015.
[4] R. Gao, Y. Jiang, and S. Abdelaziz, "All-fiber magnetic field sensors based on magnetic fluid-filled photonic crystal fibers," *Opt Lett*, vol. 38, no. 9, pp. 1539–1541, May. 2013.
[5] X. Li and H. Ding, "All-fiber magnetic-field sensor based on microfiber knot resonator and magnetic fluid," *Opt Lett*, vol. 37, no. 24, pp. 5187–5189, Dec. 2012.
[6] J. Zhang, X. Qiao, R. Wang, F. Chen, and W. Bao, "Highly sensitivity fiber-optic vector magnetometer based on two-mode fiber and magnetic fluid," *IEEE Sensors J*, vol. 19, no. 7, pp. 2576–2580, Apr. 2019.
[7] Z. Jiang *et al.*, "High-sensitivity vector magnetic field sensor based on side-polished fiber plasmon and ferrofluid," *Opt Lett*, vol. 43, no. 19, pp. 4743–4746, Oct. 2018.

[8] J. Yin *et al.*, "All-fiber-optic vector magnetometer based on anisotropic magnetism-manipulation of ferromagnetism nanoparticles," *Appl. Phys. Lett.*, vol. 110, no. 23, pp. 231104-1–231104-5, Mar. 2017.
[9] E. Fujiwara, L. E. da Silva, T. D. Cabral, H. E. de Freitas, Y. T. Wu, and C. M. d. B. Cordeiro, "Optical fiber specklegram chemical sensor based on a concatenated multimode fiber structure," *J. Lightw. Technol.*, vol. 37, no. 19, pp. 5041–5047, Oct. 2019.
[10] W. B. Spillman, B. R. Kline, L. B. Maurice, and P. L. Fuhr, "Statistical-mode sensor for fiber optic vibration sensing uses," *Appl Opt*, vol. 28, no. 15, pp. 3166–3176, Aug. 1989.
[11] L. Rodriguez-Cobo, M. Lomer, A. Cobo, and J.-M. Lopez-Higuera, "Optical fiber strain sensor with extended dynamic range based on specklegrams," *Sensors Actuators, A, Phys*, vol. 203, pp. 341–345, Dec. 2013.
[12] M. J. Murray, A. Davis, C. Kirkendall, and B. Redding, "Speckle-based strain sensing in multimode fiber," *Opt. Exp.*, vol. 27, no. 20, pp. 28494–28506, Sep. 2019.
[13] W. Chen, F. Feng, D. Chen, W. Lin, and S.-C. Chen, "Precision non-contact displacement sensor based on the near-field characteristics of fiber specklegrams," *Sensors Actuators, A, Phys*, vol. 296, pp. 1–6, Jun. 2019.
[14] E. Fujiwara, Y. T. Wu, and C. K. Suzuki, "Vibration-based specklegram fiber sensor for measurement of properties of liquids," *Opt. Lasers Eng.*, vol. 50, no. 12, pp. 1726–1730, Dec. 2012.
[15] J. J. Wang, S. C. Yan, Y. P. Ruan, F. Xu, and Y. Q. Lu, "Fiber-Optic point-based sensor using specklegram measurement," *Sensors*, vol. 17, no. 10, pp. 2429-1–2429-9, Oct. 2017.
[16] Y. Liu, G. Li, Q. Qin, Z. Tan, M. Wang, and F. Yan, "Bending recognition based on the analysis of fiber specklegrams using deep learning," *Opt. Laser Technol.*, vol. 131, pp. 106424-1–106424-6, Jun. 2020.
[17] E. Fujiwara, Y. T. Wu, M. F. M. dos Santos, E. A. Schenkel, and C. K. Suzuki, "Development of a tactile sensor based on optical fiber specklegram analysis and sensor data fusion technique," *Sensors Actuators, A, Phys*, vol. 263, pp. 677–686, Jul. 2017.
[18] F. Feng, W. Chen, D. Chen, W. Lin, and S.-C. Chen, "In-situ ultrasensitive label-free DNA hybridization detection using optical fiber specklegram," *Sensors Actuators, B, Chem*, vol. 272, pp. 160–165, Nov. 2018.
[19] L. Rodriguez-Cobo, M. Lomer, and J.-M. Lopez-Higuera, "Fiber specklegram-multiplexed sensor," *J. Lightw. Technol.*, vol. 33, no. 12, pp. 2591–2597, Jun. 2015.
[20] Z. Ding and Z. Zhang, "2D tactile sensor based on multimode interference and deep learning," *Opt. Laser Technol.*, Nov. 2020.
[21] E. Fujiwara, Y. T. Wu, M. F. M. Santos, E. A. Schenkel, and C. K. Suzuki, "Optical fiber specklegram sensor for measurement of force myography signals," *IEEE Sensors J*, vol. 17, no. 4, pp. 951–958, Feb. 2017.
[22] M. Y. Darsht, I. V. Zhirgalova, B. Y. Zel'Dovich, and N. D. Kundikova, "Observation of a 'magnetic' rotation of the speckle of light passed through an optical fiber," *JETP Lett.*, vol. 59, no. 11, pp. 734–736, Jun. 1994.
[23] L. I. Ardasheva, M. O. Sadykova, N. R. Sadykov, and V. E. Chernyakov, "Rotation of the speckle pattern in a low-mode optical fiber in a longitudinal magnetic field," *J. Opt. Techno.*, vol. 69, no. 7, pp. 451–453, Jul. 2002.
[24] D. A. Kuzmin, I. V. Bychkov, and V. G. Shavrov, "Influence of graphene coating on speckle-pattern rotation of light in gyrotropic optical fiber," *Opt Lett*, vol. 40, no. 6, pp. 890–893, Mar. 2015.
[25] F. T. Yu, M. Wen, S. Yin, and C. M. Uang, "Submicrometer displacement sensing using inner-product multimode fiber speckle fields," *Appl Opt*, vol. 32, no. 25, pp. 4685–4689, Sep. 1989.
[26] P. J. Kajenski, P. L. Fuhr, and D. R. Huston, "Mode coupling and phase modulation in vibrating waveguides," *J. Lightw. Technol.*, vol. 10, no. 9, pp. 1297–1301, Sep. 1992.
[27] M. Plöschner, T. Tyc, and T. ˇCižmár, "Seeing through chaos in multimode fibres," *Nat. Photon.*, vol. 9, no. 8, pp. 529–535, Aug. 2015.
[28] D. E. B. Flaes, J. Stopka, S. Turtaev, J. F. De Boer, T. Tyc, and T. Cizmar, "Robustness of light-transport processes to bending deformations in graded-index multimode waveguides," *Phys. Rev. Lett.*, vol. 120, no. 23, pp. 233901-1–233901-5, Jun. 2018.
[29] N. Borhani, E. Kakkava, C. Moser, and D. Psaltis, "Learning to see through multimode fibers," *Optica*, vol. 5, no. 8, pp. 960–966, Aug. 2018.
[30] E. Fujiwara, Y. Ri, Y. T. Wu, H. Fujimoto, and C. K. Suzuki, "Evaluation of image matching techniques for optical fiber specklegram sensor analysis," *Appl Opt*, vol. 57, no. 33, pp. 9845–9854, Nov. 2018.
[31] B. Redding, S. M. Popoff, and H. Cao, "All-fiber spectrometer based on speckle pattern reconstruction," *Opt. Exp.*, vol. 21, no. 5, pp. 26127–26134, Mar. 2013.
[32] V. H. Arístizabal, F. J. Vélez, E. Rueda, N. D. Gómez, and J. A. Gómez, "Numerical modeling of fiber specklegram sensors by using finite element method (FEM)," *Opt. Exp.*, vol. 24, no. 24, pp. 27225–27238, Nov. 2016.
[33] S. Qian, Y. Xu, L. S. Zhong, and L. Su, "Investigation on sensitivity enhancement for optical fiber speckle sensors," *Opt. Exp.*, vol. 24, no. 10, pp. 10829–10840, May 2016.
[34] L. P. Feng *et al.*, "Generation of LP 11/LP 21 modes with tunable mode lobe orientation controlled by polarization states," *Opt. Exp.*, vol. 27, no. 9, pp. 13150–13159, Apr. 2019.
[35] Y. Q. Fan, G. Wu, W. T. Wei, Y. F. Yuan, F. Lin, and X. Wu, "Fiber-optic bend sensor using LP 21 mode operation," *Opt. Exp.*, vol. 20, no. 24, pp. 26127–26134, Nov. 2012.
[36] J. H. Chen, D. R. Li, and F. Xu, "Optical microfiber sensors: Sensing mechanisms, and recent advances," *J. Lightw. Technol.*, vol. 37, no. 11, pp. 2577–2589, Jun. 2019.
[37] H. Liu, H. Zhang, B. Liu, B. Song, J. Wu, and L. Lin, "Ultra-sensitive magnetic field sensor with resolved temperature cross-sensitivity employing microfiber-assisted modal interferometer integrated with magnetic fluids," *Appl. Phys. Lett.*, vol. 109, no. 4, pp. 042402-1–042402-5, Jul. 2016.
[38] E. Fujiwara, M. F. Marques Dos Santos, and C. K. Suzuki, "Optical fiber specklegram sensor analysis by speckle pattern division," *Appl Opt*, vol. 56, no. 6, pp. 1585–1590, Feb. 2017.
[39] C. M. B. Cordeiro, T. H. R. Marques, L. Evaristo da Silva, and E. Fujiwara, "Polymer optical fiber specklegram strain sensor with extended dynamic range," *Opt. Eng.*, vol. 57, no. 11, pp. 116107-1–116107-9, Nov. 2018.

Run-ze Zhu received the B.Sc. degree from the Dalian University of Technology, Dalian, China, in 2019. He is currently working toward the Ph.D. degree with the College of Engineering and Applied Sciences, Nanjing University, Nanjing, China. His research interests include fiber sensing and imaging.

Sheng-jie Wan received the B.Sc. degree in materials science from Nanjing University, Nanjing, China, in 2019. He is currently working toward the Graduation degree with the College of Engineering and Applied Sciences, Nanjing University. His research focuses on microfiber devices and their applications in sensing.

Yi-feng Xiong received the B.Eng. degree in materials physics from Nanjing University, Nanjing, China. He is currently working toward the Ph.D. degree with the College of Engineering and Applied Sciences, Nanjing University, under the supervison of professor Fei Xu. His current research focuses on integrated optical fiber devices.

Hao-gong Feng received the B.Sc. degree from Nankai University, Tianjin, China, in 2019. He is currently working toward the Ph.D. degree with the College of Engineering and Applied Sciences, Nanjing University, Nanjing, China. His research focuses on fiber devices and their applications in sensing and imaging.

Ye Chen received the Ph.D. degree from Nanjing University, Nanjing, China, in 2015. He is currently an Associate Researcher with the College of Engineering and Applied Sciences, Nanjing University. His research focuses on optical fiber or microfiber devices and their applications.

Yan-qing Lu received the Ph.D. degree from Nanjing University, Nanjing, China, in 1996. He is currently a Professor with the College of Engineering and Applied Sciences, Nanjing University. His research interests include nanophotonics and liquid crystal devices.

Fei Xu received the Ph.D. degree from the Optoelectronics Research Center, University of Southampton, Southampton, U.K., in 2008. He is currently a Professor with the College of Engineering and Applied Sciences, Nanjing University, Nanjing, China. His research focuses on fiber optics.